Magnesium Monocationic Complexes: A Theoretical Study of Metal Ion Binding Energies and Gas-Phase Association Kinetics

Robert C. Dunbar*

Chemistry Department, Case Western Reserve University, Cleveland, Ohio 44106

Simon Petrie*

Department of Chemistry, The Faculties, Australian National University, Canberra ACT 0200, Australia

Received: July 21, 2004; In Final Form: October 25, 2004

Bond dissociation energies (BDEs) for complexes of ground state Mg^+ (^2S) with several small oxygen- and nitrogen-containing ligands (H_2O, CO, CO_2, H_2CO, CH_3OH, HCOOH, H_2CCO, CH_3CHO, c-C_2H_4O, H_2CCHOH, CH_3CH_2OH, CH_3OCH_3, NH_3, HCN, H_2CNH, CH_3NH_2, CH_3CN, $CH_3CH_2NH_2$, $(CH_3)_2NH$, H_2NCN, and $HCONH_2$) have been calculated at the CP-dG2thaw level of theory. These BDE values, as well as counterpoise-corrected MP2(thaw)/6-311+G(2df,p) calculations on the Mg^+ complexes of several larger ligands, augment and complement existing experimental or theoretical determinations of gas-phase Mg^+/ligand bond strengths. The reaction kinetics of complex formation are also investigated via variational transition state theory (VTST) calculations using the computed ligand and molecular ion parameters. Radiative association rate coefficients for most of these systems increase by approximately 1 order of magnitude with every 3-fold reduction in temperature from 300 to 10 K. Several of the largest molecules surveyed—notably, CH_3COOH, $(CH_3)_2CO$, and CH_3CH_2CN—exhibit comparatively efficient radiative association with Mg^+ ($k_{RA} \geq 1.0 \times 10^{-10}$ cm^3 molecule^{-1} s^{-1}) at temperatures as high as 100 K, implying that these processes may have a considerable influence on the metal ion chemistry of warm molecular astrophysical environments known to contain these potential ligands. Our calculations also identify the infrared chromophoric brightness of various functional groups as a significant factor influencing the efficiency of the radiative association process.

1. Introduction

The study of gas-phase metal ion complexation by various inorganic and organic ligands has been a mainstay of mass spectrometric research since at least the 1970s.[1−5] Ongoing research in this field promotes our understanding of many aspects of metal ion coordination chemistry, such as the involvement of metal ions in diverse biochemical processes,[6−10] the fundamental bond strengths of individual metal ion/ligand bonds,[11−16] the influence of solvation on metal ion chemistry and reactivity,[17−19] and even the speciation of metals within cold astrophysical environments.[20−22]

Increasingly, the efforts of experimentalists to explore gas-phase metal ion chemistry have been matched by the implementation of quantum chemical methods, and other theoretical approaches, to explore particular properties of metal-containing ions. Sophisticated computational techniques can prove particularly useful in investigating processes (e.g., radiative association reactions of metal ions with ligands, at very low temperature and pressure) which are especially elusive to experimental pursuit. In this context, some of the association processes investigated here ($Mg^+ + H_2O$, CO, NH_3 and HCN) have been examined in an earlier variational transition state theory (VTST) study[23] which focused on likely loss processes for main-group metal ions within interstellar clouds. These association reactions are reevaluated here because the CP-dG2thaw computational approach used in the present work[24,25] to evaluate Mg^+/ligand BDEs is expected to offer significantly improved accuracy over the theoretical method used in the earlier work.

Although the magnesium ion's water,[26−34] methanol,[27,34−38] and ammonia[26,34,39−42] complexes in particular have received considerable attention due to the importance of these ligands as solvents, the Mg^+ chemistry of several of the larger ligands here (including formic acid, dimethyl ether, ethylene oxide, and cyanamide) has not been subjected to any previous theoretical or experimental study. The present work thus complements and extends recent efforts to characterize Mg^+ binding energies to a wide variety of ligands.[34,36,40,41,43]

Metal ion/ligand binding energy determinations have a broad general utility. Beyond such considerations, an additional motivation for the study of Mg^+ complexation to the oxygen- and nitrogen-bearing bases surveyed here is, as acknowledged above, to enhance our understanding of the chemistry of cold astrophysical environments. The formation of MgNC within carbon-rich outflowing circumstellar envelopes,[44,45] protoplanetary nebulae,[46] and perhaps also cold dense interstellar clouds, is thought to occur via radiative association of Mg^+ to the cyanopolyynes $HC_{2n+1}N$ ($n = 0-5$).[47] Although cyanopolyynes dominate the detectable large molecules found in the regions within which MgNC has been found, they are not a major feature of the chemical evolution within warmer giant molecular clouds and star-forming regions.[48−51] Instead, the most promising potential ligands within the latter environments are less highly unsaturated organic molecules featuring amine, alcohol, ether, carbonyl, or carboxylic functional groups. Almost all of the ligands surveyed in the present work have been detected in one or more "warm" ($T \sim 50-200$ K) interstellar environments. The recent discovery of a gas-phase metal-containing molecule,

10.1021/jp046777m CCC: $30.25
Published on Web 01/27/2005

FeO, in such an environment[52,53] prompts questions concerning the speciation of other metals in these regions.[54] To assess what role, if any, Mg^+ plays in the chemical evolution of giant molecular clouds or star-forming regions, and to guide detection efforts toward the most probable Mg-containing neutrals arising under these conditions, an essential step is to establish the efficiencies of the various possible Mg^+/ligand radiative association reactions. The VTST calculations reported here use a well-established method for making such estimates.

2. Theoretical Methods

2.1. Ab Initio Quantum Chemical Calculations. Optimized geometries and harmonic vibrational frequencies were obtained via hybrid density functional theory (DFT), at the B3-LYP/6-311+G** level of theory. This combination of Becke's 3-parameter exchange functional (B3)[55] with the Lee−Yang−Parr (LYP) correlation functional[56] is widely regarded as an efficient and reliable method for determining the structural and spectroscopic details which characterize small molecules and molecular ions. Magnesium ion/ligand bond dissociation energy (BDE) values were calculated using the B3-LYP/6-311+G** optimized geometries and (unscaled) zero-point vibrational energies in conjunction with a sequence of single-point total energy calculations according to the CP-dG2thaw protocol.[24,25] The latter procedure is adapted from standard Gaussian-2 (G2) theory[57] but departs from the G2 procedure in its assignment of the correlation space for the metal atom,[58] in the largest metal atom basis set used,[25] and in its inclusion of a counterpoise correction for the metal ion/ligand bond.[24,59] A more detailed description of, and justification for, these modifications has been presented previously.[24,25,58,60]

All calculations were performed using the GAUSSIAN98 quantum chemistry suite of programs.[61]

2.2. VTST Association Rate Coefficient Calculations. Variational transition state theory (VTST) has been used as a convenient approach to estimating radiative association rate coefficients with an accuracy approaching the limits of the assumptions inherent in transition state theory.[62] The noncovalent nature of the complexes and the large intermolecular separations at the transition states in these systems are features making it likely that transition state theory gives an accurate account of the kinetics. The strong attractive forces arising from the charge-polarizability (spherically averaged) and ion−dipole interactions were included in the intermolecular potential energy function used here. Various shorter range attractive and repulsive terms have been found to have no significant effect on the kinetics of interest here even in the most demanding cases (which are reactions of long, polar molecules such as the cyanopolyynes)[63] and were not included in the potential energy function. The molecular quantities needed as inputs for the VTST calculation are available from the quantum-chemical results with sufficient accuracy and confidence for the kinetic estimates needed in astrochemical modeling studies. The VariFlex kinetics package[64] to implement the VTST approach was used as has been described in our previous publications.[23,63]

3. Results and Discussion

3.1. Calculation and Assessment of BDE Results. Our CP-dG2thaw calculations of Mg^+/ligand BDE values are summarized in Table 1, which also includes representative literature values for comparison. As an adjunct to the CP-dG2thaw calculations, we provide also BDE values determined using the less demanding method CP-MP2(thaw)/6-311+G(2df,p)//B3-LYP/6-311+G**, hereafter abbreviated CP-MP2(thaw). We have also used CP-MP2(thaw) to calculate BDE values for several ligands too large for convenient treatment using CP-dG2thaw.

TABLE 1: Mg^+/Ligand BDEs Calculated at the CP-MP2(thaw)/6-311+G(2df,p) and CP-dG2thaw Levels of Theory

	BDE/kJ mol^{-1}			
	this work		lit.	
ligand[a]	CP-MP2	CP-dG2thaw	expt	theor
H_2*O*	119.6[b]	121.7[b]	119(13)[c]	135,[d] 131,[e] 118,[f] 119[g]
*C*O	40.6	41.7	42(6)[c]	42[g]
H_2C*O*	122.7	128.9		
CH_3*O*H	139.9	144.3	146(7)[c]	149,[e] 142[g]
*O*CO	53.9	60.7	58(6)[c]	54[g]
HC*O*OH[h,i]	135.8	143.0		
H_2CC*O*	84.9	96.1		
CH_3CH*O*	151.6	157.8	155(7)[j]	
c−C_2H_4*O*	147.8	153.6		
H_2CCH*O*H	113.9	121.8		
CH_3CH_2*O*H	151.0	155.5	153(7)[j]	
CH_3*O*CH_3	148.9	154.8		
CH_3C*O*OH[h,k]	157.6			
HC*O*OCH_3[h,l]	155.3			
HC*O*CH_2O*H*[m]	211.4			
CH_3C*O*CH_3	173.7		173(7)[j]	
HC*O*NH_2	193.3	199.1		203.3[n]
NH_3	150.6[b]	151.1[b]	154(12)[c]	158,[d] 149[g]
HC*N*	128.7[o]	129.4[o]		
H_2CNH	162.0	162.9		
CH_3N*H*$_2$	165.3	167.4		
CH_3CN	168.9	163.0		
NH_2CN[h,p]	187.2	186.3		
CH_3CH_2N*H*$_2$	173.8	175.8		
$(CH_3)_2N$H	172.3	175.9		
HC_5N	161.2[o]	160.6[o]		
CH_2CHCN	152.8			
CH_3CH_2CN	175.5			
HC_7N	165.8[o]			

[a] Italicized atom(s) indicate site(s) of direct coordination to Mg^+. [b] Previously reported in ref 72. [c] Collision-induced dissociation measurement, ref 34. [d] MCPF/TZP calculation, ref 26. [e] SCF/TZP calculation, ref 27. [f] CCSD(T)/6-311++G(2df,p) calculation, ref 33. [g] MP2/6-311+G(2d,2p) calculation, ref 34. [h] A second, higher energy isomeric complex has also been identified. [i] BDE(Mg^+−HCO*O*H) = 66.7 kJ mol^{-1} (CP-MP2), 71.3 kJ mol^{-1} (CP-dG2thaw). [j] FT-ICR equilibrium measurement, ref 35; reassigned by Andersen et al. (ref 34). [k] BDE(Mg^+−CH_3C*O*OH) = 87.1 kJ mol^{-1} (CP-MP2). [l] BDE(Mg^+−HCO*O*CH_3) = 81.3 kJ mol^{-1} (CP-MP2). [m] Additional isomeric complexes have been identified. BDE(Mg^+−HC*O*CH_2OH) = 143.9 kJ mol^{-1} (CP-MP2), BDE(Mg^+−HCOCH_2*O*H) = 138.1 kJ mol^{-1} (CP-MP2). [n] G2(MP2) calculation, ref 70. [o] Previously reported in ref 73. [p] BDE(Mg^+−*N*H_2CN) = 58.5 kJ mol^{-1} (CP-MP2), 62.3 kJ mol^{-1} (CP-dG2thaw).

There is a clear disparity between the performance of the two computational methods (CP-MP2(thaw) and CP-dG2thaw) that depends on the identity of the formal donor atom within the Mg^+/ligand complex. For O-coordinated complexes, the more CPU-intensive CP-dG2thaw method consistently delivers BDE values exceeding those determined using CP-MP2(thaw), with a mean discrepancy of 6.2 kJ mol^{-1} and standard deviation of 2.2 kJ mol^{-1}.[65] Conversely, for N-coordinated ligands the mean absolute discrepancy between the two methods is only 0.4 kJ mol^{-1} (standard deviation = 2.9 kJ mol^{-1}). Over the set of N-coordinated ligands covered by both computational methods there are two species, CH_3CN and H_2NCN, for which the less expensive CP-MP2(thaw) method actually gives the larger BDE.

Comparison of our calculated values with literature measurements shows generally very good agreement with recent

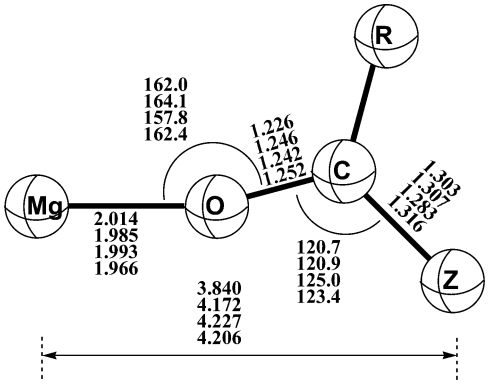

Figure 1. Diagram of key geometric parameters for the lowest energy structures found for complexes of Mg^+ with HCOOH, CH_3COOH, $HCOOCH_3$, and $HCONH_2$ at the B3-LYP/6-311+G** level of theory. Bond lengths in angstroms and bond angles in degrees are shown in order for these four complexes. In all cases, the coordinated "O" atom is the carbonyl oxygen and "Z" is the other potential (O or N) donor atom. Also shown is the internuclear distance between Mg and Z. Optimized values of the ∠(MgOCZ) dihedral angle are 0° for HCOOH and 180° for the three larger ligands.

experimental studies. Armentrout and co-workers[34,66] have used collision-induced dissociation (CID) to determine Mg^+ BDE values for H_2O, CO, CO_2, CH_3OH, and NH_3, with agreement within ±6 kJ mol^{-1} seen for the CP-dG2thaw values for all of these ligands. The measurement for CO_2 is of particular interest: here the CP-MP2(thaw) value, 6.8 kJ mol^{-1} below CP-dG2thaw, is clearly at odds with the CID measurement of 58 ± 6 kJ mol^{-1},[34] as well as with a photodissociation study yielding BDE = 62 kJ mol^{-1}.[67] The substantially better agreement with experiment seen here for CP-dG2thaw versus CP-MP2(thaw) is in accordance with expectations that the more computationally demanding CP-dG2thaw method should offer a more reliable description of the metal/ligand interaction. Good agreement with our calculations is also seen for the *relative* BDE values obtained for CH_3OH, CH_3CHO, C_2H_5OH, and CH_3COCH_3 by Operti et al.[35] using several ion-chemistry strategies in the Fourier transform ion cyclotron resonance (FT-ICR) mass spectrometer. Large discrepancies are evident with the *absolute* BDE values reported in the latter study.[35] The absolute values determined by Operti et al.[35] were anchored to measurements of the photodissociation (PD) thresholds for the Mg^+ complexes of CH_3OH and CH_3COCH_3. In keeping with our own findings, such PD-derived bond strengths have been inferred by several authors to be systematically much too large in many instances and should not be considered to be reliable thermochemical anchors.[34,68]

A notable structural feature arising from our calculations is that, of 7 ligands containing a pair of potential σ-donor atoms (CO_2, HCOOH, CH_3COOH, $HCOOCH_3$, $HCOCH_2OH$, $HCONH_2$, and H_2NCN), only $HCOCH_2OH$ can be considered to produce a truly bidentate Mg^+/ligand complex as the most strongly bound adduct. The inability of linear CO_2 to chelate Mg^+ is comprehensible on geometric grounds, and a similar impediment to simultaneous coordination of the amide and nitrile functionalities of H_2NCN can also be expected.

The failure of chelation by HCOOH, CH_3COOH, $HCOOCH_3$, and $HCONH_2$ is more surprising. Preferred geometries for these four complexes are shown in Figure 1. In all four cases, the sole coordination site is the carbonyl O atom.[69] Higher energy local minima are also identifiable for the carboxylate ligands (see Table 1), but not for formamide; these other local minima feature comparatively weak (BDE < 90 kJ mol^{-1}) monodentate coordination to the sp^3 O atom. All efforts to isolate chelating geometries for these species were unsuccessful, collapsing to one or other of the identified monodentate complexes. One possible rationalization of the preference for nonchelating carbonyl O coordination in these complexes can be made in terms of the ability of all of these molecules to rehybridize the non-carbonyl heteroatom (Z), giving a contribution from a resonance structure with partial double-bond character to the C−Z bond, and partial positive charge on Z. For formamide, for example, this is a resonance form $O^-{-}C(H){=}N^+H_2$. Attaching the Mg^+ to this molecular structure gives a covalently bonded, ligand-ionized resonance form $MgO{-}C(H){=}N^+H_2$. Examination of the optimized geometries for these four complexes does in some measure support the notion that such a resonance form contributes to the stability of the observed structures. Although the carbonyl C−O bond, in each of the four identified complexes, is lengthened by about 0.03 Å on coordination to Mg^+, the effect on the neighboring C−Z bond (where Z is the nominally sp^3-hybridized O or N atom of the carboxylate or amide functional group) is rather more pronounced: this bond is typically contracted by ∼0.05 Å, which would correspond to increasing double-bond character.

We have pursued an "atoms-in-molecules" (AIM) analysis[74] of bonding and atomic charges to gauge the validity of the above rationale for nonchelation in the carboxylate and formamide ligands. This analysis is summarized in Table 2. In all complexes, addition of Mg^+ results in a modest covalent $Mg^+{-}X$ interaction, where X is the donor atom: the effective atomic charge on Mg is between 0.94 and 1.02 unit positive charges; the localized spin density on Mg is between 0.89 and 0.93 unpaired electrons; and the $Mg^+{-}X$ covalent bond order is between 0.23 and 0.34. The highest apparent degree of covalency exists in the Mg^+/amine complexes, which have the lowest Mg^+ effective charges (and upaired spin densities) and the greatest metal−ligand covalent bond orders, but the range in values for any of these parameters is rather limited and does not seem to follow a systematic dependence on the computed BDE. In all O- and N-coordinating complexes, Mg^+ coordination yields a significant decrease in the covalent bond order for the X−Y bond, where Y is the donor (X) atom's nearest nonhydrogenic neighbor. The covalent Y−Z bond order, where Z is the next nearest neighbor, is most significantly enhanced (Δ_{BO}(Y−Z) ≥ 0.09) in the cases where Z is also O or N (i.e, the four "nonchelaters" discussed above, as well as H_2NCN and CO_2). The Y−Z bond order is mildly enhanced on complexation (Δ_{BO}(Y−Z) = 0.03−0.07) in the ligands featuring conjugated π systems (H_2CCO, H_2CCHOH, and H_2CCHCN), and only weakly affected by complexation (Δ_{BO}(Y−Z) = 0.01−0.06) when only a σ-bonded carbon backbone is present. These trends in calculated Y−Z bond order point toward stabilization of the nonchelating form of the complex by the suggested covalent resonance form in the carboxylate, formamide, cyanamide and carbon dioxide ligands. This description is also consistent with the otherwise curious geometric feature (see Figure 1) exhibited by the 180° ∠MgOCZ dihedral seen for the acetic acid, methyl formate, and formamide complexes, which ensures that the potential second donor atom "Z" is located about as far as possible from the Mg^+ ion.

In contrast to these cases, the ligand glycolaldehyde, $HCOCH_2OH$, is found to favor the chelating form of the complex. The Mg−O bond lengths of 2.17 Å (alcohol O) and 2.14 Å (carbonyl O) show that in this complex, the binding of Mg^+ is essentially evenhanded. A similar degree of metal/ligand covalency as for the nonchelating complexes discussed above is suggested by the Mulliken charge of 0.69 determined for Mg in the $HCOCH_2$-

TABLE 2: Atoms-in-Molecules (AIM) Properties of Ligands and Mg^+/Ligand Complexes, at the B3-LYP/6-311+G Level of Theory**

	atomic charges[a]				bond orders[c]				
ligand	q(Mg)	$q(X)_{Mg}$	q(X)	$\rho_{spin}(Mg)$[b]	(Mg−X)	$(X-Y)_{Mg}$	(X−Y)	$(Y-Z)_{Mg}$	(Y−Z)
H_2O	1.01	−1.28	−1.10	0.91	0.30				
CO	0.98	1.04	1.14	0.93	0.23	1.88	1.82		
H_2CO	1.00	−1.24	−1.06	0.93	0.27	1.42	1.58		
CH_3OH	1.00	−1.22	−1.06	0.91	0.30	0.85	0.94		
OCO	1.02	−1.24	−1.07	0.92	0.24	1.36	1.56	1.66	1.56
HCOOH	0.99	−1.29	−1.11	0.93	0.28	1.24	1.46	1.05	0.96
H_2CCO	1.00	−1.26	−1.08	0.93	0.26	1.39	1.61	1.91	1.84
CH_3CHO	0.99	−1.28	−1.09	0.93	0.29	1.34	1.53	1.10	1.04
H_2CCHOH	1.00	−1.23	−1.08	0.91	0.29	0.86	0.98	1.90	1.87
CH_3CH_2OH	0.99	−1.22	−1.06	0.90	0.29	0.82	0.91	1.03	1.00
CH_3OCH_3	0.99	−1.18	−1.04	0.91	0.29	0.85	?[d]		
CH_3COOH	0.98	−1.33	−1.15	0.93	0.29	1.17	1.41	1.02	0.93
$HCOOCH_3$	0.98	−1.31	−1.13	0.93	0.30	1.20	1.44	1.10	0.98
CH_3COCH_3	0.98	−1.31	−1.11	0.93	0.30	1.28	1.49	1.06	1.02
$HCONH_2$	0.98	−1.32	−1.14	0.93	0.31	1.19	1.43	1.29	1.15
NH_3	0.96	−1.19	−1.00	0.90	0.33				
HCN	0.98	−1.33	−1.09	0.93	0.26	2.35	2.53		
H_2CNH	0.96	−1.30	−1.06	0.91	0.32	1.66	1.78		
CH_3NH_2	0.95	−1.16	−0.97	0.89	0.34	0.97	1.04		
CH_3CN	0.97	−1.40	−1.14	0.93	0.28	2.27	2.48	1.10	1.08
NH_2CN	0.96	−1.36	−1.10	0.93	0.29	2.23	2.47	1.34	1.22
$CH_3CH_2NH_2$	0.94	−1.16	−0.97	0.89	0.34	0.94	1.02	1.03	1.02
$(CH_3)_2NH$	0.94	−1.15	−0.96	0.89	0.33	0.97	1.03		
CH_2CHCN	0.96	−1.39	−1.10	0.93	0.29	2.25	2.46	1.15	1.12
CH_3CH_2CN	0.96	−1.42	−1.14	0.93	0.29	2.25	2.47	1.07	1.06

[a] Effective atomic charge on complexed Mg^+ or on the "donor atom" X. The two values shown for atom X apply respectively to the complexed and the free ligand. [b] Localized metal atom spin density on complexed Mg^+. [c] Calculated covalent bond orders for key bonds within the complex and the free ligand. X is the donor atom, Y its nearest (non-hydrogenic) neighbor atom, and Z the next nearest (non-hydrogenic) neighbor. (In ligands presenting a choice of next-nearest neighbor, Z is preferentially the remaining O or N atom, or sp^2-hybridized C atom). For the X−Y and Y−Z bonds, the two values shown in each instance apply respectively to the complexed and the free ligand. [d] AIM calculation of this parameter could not be executed correctly due to strong zero-flux surface curvature.

OH adduct. However, here the ligand's intervening CH_2 moiety does not readily permit the type of resonance delocalization postulated for the carboxylate and amide complexes. Although this sole chelating complex is notable as the most strongly bound adduct of those surveyed within Table 1 (with a BDE 18.1 kJ mol^{-1} larger than that of formamide according to our CP-MP2 calculations), it can be noted that the BDE for Mg^+/glycolaldehyde is approximately 40 kJ mol^{-1} lower than the sum of the BDEs for a small aldehyde, such as H_2CO, and a small alcohol, such as CH_3OH. Furthermore, we have also located local minima (Table 1) in which the ligand's conformation permits coordination to one or other O atom, but not both. In the two such local minima identified, monodentate coordination to either the carbonyl or the hydroxyl O atom gives a BDE of ~140 kJ mol^{-1} at the CP-MP2 level of theory. Thus chelation delivers a BDE approximately 70 kJ mol^{-1} weaker than the sum of the individual donor atom terms. Clearly, the energetic contributions to coordination of individual donor atoms within a chelating ligand do not obey a strict addivitity.

Finally, an anonymous referee has noted that the identification of a chelating geometry for glycolaldehyde, but not for the carboxylate ligands nor for formamide, conforms with the condensed-phase "folk rule" which states that chelation is preferred when it permits formation of a five- or six-membered ring, but not for smaller or larger ring sizes. The ring-size rule is generally applied to transition metal complexation where the metal−ligand interaction is often dominated by covalent or coordinate covalent bonding, and for which the concept of angle strain is comparatively meaningful. In the present study, the complexes in question have only a modest contribution from electron sharing in the metal−ligand interaction, so considerations of strain at the metal site are likely not highly relevant. Further, the preferred geometry seen in most of the "failed chelate" complexes (Figure 1) is more consistent with a distinct electrostatic preference for monodentate coordination than with a frustrated drive toward chelation in these complexes.

3.2. Ligation of Mg^+ versus Na^+ and Mg^{2+}: Trends and Preferences. Use of the CP-dG2thaw method in the present work allows direct comparison of our Mg^+ calculations with the ligand binding energies determined for Na^+ [24] at the same level of theory. A graph comparing these values is shown in Figure 2. Though there is a generally consistent trend for the BDEs of both metal ions to increase with increasing ligand size, it is clear that the relationship between Na^+ and Mg^+ BDEs is not a perfectly linear one. The BDEs for Na^+ and Mg^+ to nonpolar CO_2 are nearly identical, and the values for CO are also a close match, as indicated by the proximity of these data points to the interpolated line of slope 1, but for all of the polar ligands BDE(Mg^+) considerably exceeds BDE(Na^+). More subtle disparities are also evident. The BDE(Na^+) value for HCN (103.2) marginally exceeds that for dimethyl ether (102.5), whereas the BDE(Mg^+) value for the latter ligand (154.8) is 25 kJ mol^{-1} larger than for the former. A distinct reversal is found for acetonitrile and dimethylamine: when competing for Na^+, the nitrile is more strongly bound by 17.1 kJ mol^{-1} [24] whereas for coordination to Mg^+ the amine wins out by 12.9 kJ mol^{-1}. Because the CP-dG2thaw method shows extremely good agreement with relative BDE values found experimentally[71] for Na^+ (and should presumably perform to a similar high standard for Mg^+), we can assert with reasonable confidence that these binding energy incongruities are genuine features reflecting particular metal ion/ligand coordination

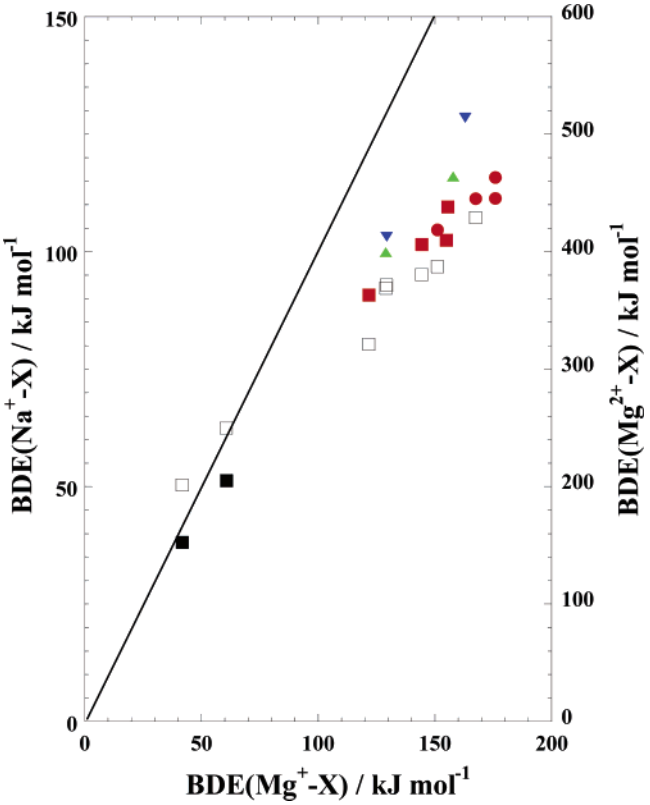

Figure 2. Graph comparing metal ion/ligand BDE values for Mg^+, obtained in the present work, with the Na^+ and Mg^{2+} values obtained for the same ligands in previous studies.[24,60] The 8 Mg^{2+} data points from Table 4 (excluding N_2) are represented by hollow squares (right-hand vertical scale), and the 12 Na^+ data points from Table 3 are variously represented in color (left-hand vertical scale) as O-coordinating polar neutrals (green triangles, sp^2-coordinated donor atom; red squares, sp^3-coordinated donor), N-coordinating polar neutrals (blue triangles, sp-coordinated donor; red circles, sp^3-coordinated donor). In addition, two Na^+ points for nonpolar neutrals CO and CO_2 are shown (black squares). In all cases, the values shown are those obtained from CP-dG2thaw calculations. The line shown, which has a slope of 1 for Na^+:Mg^+ (and 4 for Mg^{2+}:Mg^+) is not intended as a fit to the data.

preferences rather than spurious effects arising from inaccuracies in the computational method.

More generally, it is notable that the four "unsaturated" polar ligands common to the Na^+ study and the present work—H_2CO, HCN, CH_3CHO, and CH_3CN—generally lie closer to the "line of unit slope" in Figure 2 than do the "saturated" polar ligands H_2O, CH_3OH, CH_3OCH_3, C_2H_5OH, NH_3, CH_3NH_2, $C_2H_5NH_2$, and $(CH_3)_2NH$. This observation might imply that Mg^+ has a particular advantage in coordinating to sp^3-hybridized σ-donors, which does not apply to their sp^2- or sp-hybridized analogues. However, the underlying basis for such a suggestion is unclear.

The entire group of *polar* ligands common to both the CP-dG2thaw study of Na^+ complexation and the present work can be compared with respect to their relative affinities for Na^+ versus Mg^+. This can be done, as shown in Table 3, either by looking at the difference in BDEs as in column 3, or by looking at the ratios of BDE's as in column 4. Either way, there is a fairly good correlation between increasing dipole moment (as calculated at the B3-LYP/6-311+G** level of theory used here to obtain optimized geometries) and decreasing Mg^+ complexation bond strength relative to Na^+, as is seen by ranking the ligands in order of dipole moment as in Table 3. However, the two "nonpolar" ligands CO and CO_2 are completely out of line with this correlation. An accurate overall statement would be

TABLE 3: Dependence of Relative Bond Strengths to Mg^+ and to Na^+ on Ligand Dipole Moment and Polarizability

ligand	μ/D[a]	ΔBDE(Mg^+)−(Na^+)[b]/ kJ mol^{-1}	BDE(Mg^+)/ BDE(Na^+)[b]	α/Å^3 [c]
$(CH_3)_2NH$	1.05	64.5	1.58	35.9
$CH_3CH_2NH_2$	1.35	60.0	1.52	35.9
CH_3NH_2	1.41	56.1	1.50	23.3
CH_3OCH_3	1.45	52.3	1.51	31.1
NH_3	1.69	46.4	1.44	11.6
CH_3CH_2OH	1.76	45.9	1.42	31.0
CH_3OH	1.89	42.7	1.42	18.7
H_2O	2.16	30.9	1.34	7.3
H_2CO	2.48	29.0	1.29	15.5
CH_3CHO	2.95	41.8	1.36	28.4
HCN	3.06	26.2	1.25	14.5
CH_3CN	4.05	34.5	1.27	26.9

[a] Dipole moment (ref 75). [b] CP-dG2thaw values, using Na^+ BDEs first reported in ref 24. [c] Static electric polarizability (ref 76, 77).

TABLE 4: Comparison of Mg^+ and Mg^{2+} Ion/Ligand BDEs

ligand	BDE/kJ mol^{-1} [a] Mg^+	BDE/kJ mol^{-1} [a] Mg^{2+} [b]	BDE(Mg^{2+})/BDE(Mg^+)
N_2	26.5[c]	167.1	6.31
CO	41.7	201.3	4.83
CO_2	60.7	249.9	4.12
H_2O	121.7	321.3	2.64
H_2CO	128.9	368.9	2.86
HCN	129.4	371.9	2.87
CH_3OH	144.3	380.6	2.64
NH_3	151.1	287.3	2.56
CH_3NH_2	167.4	429.1	2.56

[a] CP-dG2thaw value (at zero K). [b] Reference 60. [c] Reference 73.

that, when compared with Na^+, Mg^+ shows a greater preference for ligands with a modest dipole moment and a large static polarizability (such as $(CH_3)_2NH$, with μ = 1.05 D and α = 35.9 Å^3 according to our calculations) than to ligands of higher dipole moment and lower polarizability (e.g., CH_3CN, with μ = 4.05 D and α = 26.9 Å^3). The characteristic of a large polarizability and weak polarity is descriptive of a "soft" base, so that these results support the notion that Mg^+ has a greater preference for soft bases (the metal ion complexes of which are expected to feature significant covalency) than does Na^+, which exhibits more purely electrostatic character in its ion/molecule complexes.

Figure 2 also displays the correlation of the monocation Mg^+ BDEs with the corresponding BDEs to the Mg^{2+} dication. The CP-dG2thaw ion/ligand BDEs of both Mg^+ and Na^+ [24] are consistently much smaller than the corresponding Mg^{2+} values.[60] The removal of the remaining 3s electron from Mg^+ reduces the effective ionic radius as well as increasing the ion's charge, and both of these factors contribute to a much greater electrostatic attraction between the magnesium dication and the ligand. In comparing the Mg^+ and Mg^{2+} BDEs,[60] we find two distinct populations among the limited set of ligands common to this work and the previous Mg^{2+} study (see Table 4). First, the nonpolar ligands CO and CO_2 (as well as N_2)[73] exhibit Mg^{2+} BDEs[60] that exceed those for Mg^+ by a factor of 4 or greater. These are the ligands with negligible propensity toward covalent Mg^+/ligand character, and consequently their interactions with both Mg^+ and Mg^{2+} are dominated by ion/ligand electrostatic attractive forces, heavily "favoring" Mg^{2+}. Second, the polar ligands H_2O, CH_3OH, H_2CO, NH_3, CH_3NH_2, and HCN have Mg^{2+}:Mg^+ BDE ratios of 2.7 ± 0.2. The reduction in the Mg^{2+}:Mg^+ BDE ratio for polar, versus nonpolar, ligands suggests that covalent character plays a significant part in the stabilization

TABLE 5: VTST Results for Radiative Association Rate Coefficients vs Temperature[a]

ligand	S^b	$E_o{}^c$	k_{assoc} (10 K)	k_{assoc} (30 K)	k_{assoc} (100 K)	k_{assoc} (300 K)
HC_7N	25	165.8	4.34E−08	1.87E−08	9.48E−09	7.6E−10
CH_3COCH_3	27	179.7	2.19E−08	7.7E−09	1.41E−09	6.08E−11
CH_3CH_2CN	24	175.5	9.4E−09	1.36E−09	1.27E−10	4.95E−12
HC_5N	19	160.6	9.06E−09	3.03E−09	6.07E−10	2.45E−11
$HCOCH_2OH$	21	217.4	6.87E−09	1.11E−09	1.11E−10	4.46E−12
CH_3COOH	21	163.6	5.51E−09	1.02E−09	1E−10	5.4E−12
$HCOOCH_3$	21	161.3	2.55E−09	3.6E−10	3.21E−11	1.41E−12
$CH_3CH_2NH_2$	27	175.8	1.57E−09	2.21E−10	1.92E−11	7.19E−13
$(CH_3)_2NH$	27	175.9	1.16E−09	1.63E−10	1.34E−11	4.58E−13
CH_3CH_2OH	24	155.5	4.7E−10	5.86E−11	4.35E−12	1.51E−13
CH_3OCH_3	24	154.8	3.47E−10	4.35E−11	3.91E−12	1.95E−13
$HCONH_2$	15	199.1	2.75E−10	3.29E−11	1.89E−12	4.21E−14
CH_3CHO	18	157.8	1.53E−10	1.87E−11	1.58E−12	9.84E−14
CH_2CHCN	18	152.8	1.36E−10	1.66E−11	1.53E−12	9.48E−14
NH_2CN	12	186.3	7.35E−11	8.76E−12	5.01E−13	1.12E−14
CH_3CN	15	163	1.2E−11	1.44E−12	1.35E−13	1.1E−14
c-C_2H_4O	18	153.6	7.36E−12	8.92E−13	8.48E−14	9.58E−15
CH_3NH_2	18	167.4	5.59E−12	6.78E−13	6.3E−14	5.51E−15
H_2CCHOH	18	121.8	3.86E−12	4.72E−13	4.54E−14	3.76E−15
$HCOOH$	12	143	2.65E−12	3.21E−13	3.05E−14	3.36E−15
CH_3OH	15	144.3	1.32E−12	1.6E−13	1.43E−14	1.12E−15
H_2CNH	12	162.9	2.04E−13	2.47E−14	2.32E−15	2.69E−16
H_2CCO	12	96.1	1.41E−13	1.71E−14	1.64E−15	1.49E−16
H_2CO	9	128.9	3.37E−14	4.1E−15	3.87E−16	4.67E−17
NH_3	9	151.1	1.48E−14	1.78E−15	1.63E−16	1.93E−17
H_2O	6	121.7	3.29E−15	3.89E−16	3.65E−17	4.34E−18
HCN	7	129.4	2.08E−15	4.29E−16	7.26E−17	1.4E−17
OCO	7	60.7	3.0E−17	8.5E−18	2.4E−18	7.6E−19
CO	4	41.7	8.09E−20	2.39E−20	6.05E−21	2.09E−21

[a] Rate coefficients, cm^3 $molec^{-1}$ s^{-1}. [b] Number of internal degrees of freedom of association complex. [c] Binding energy, kJ mol^{-1}.

of the magnesium monocation's complexes with polar ligands. Furthermore, the preference of Mg^+ for moderately polar ligands of high intrinsic polarizability is also reflected in the tendency for the saturated organics (and H_2O and NH_3) toward lower Mg^{2+}:Mg^+ BDE ratios than those of the unsaturated organics H_2CO and HCN. Finally, it is notable that the Mg^{2+}:Mg^+ BDE ratios of 2.64 for both H_2O and CH_3OH, 2.56 for both NH_3 and CH_3NH_2, and 2.86−2.87 for H_2CO and HCN display such high "internal consistency" within the apparent compound classes of saturated O-donors, saturated N-donors, and unsaturated polar organics. These values suggest that it may be possible, for example, to accurately predict the Mg^{2+} affinities of larger O-containing saturated organics solely on the basis of measured (or calculated) values for the corresponding Mg^+ complexes. However, the small number of ligands surveyed in Table 4 is insufficient to substantiate this possibility at present.

3.3. VTST Calculations of Metal Ion/Ligand Radiative Association Kinetics. The calculated association rate coefficients are shown in Table 5. The context of the kinetic modeling[23,62,63,78] is the association reaction sequence

$$M^+ + \text{ligand} \underset{k_b}{\overset{k_f}{\rightleftharpoons}} M^+(\text{ligand})^* \xrightarrow{k_r} M^+(\text{ligand}) \qquad (1)$$

The overall rate coefficient k_{assoc} for radiative association is jointly governed by the three microscopic rate coefficients in this equation. The rate coefficient k_f for formation of the metastable complex is similar to the collision rate and does not vary greatly from system to system, usually lying near 10^{-8} cm^3 $molecule^{-1}$ s^{-1} at low temperature. The rate coefficient k_r for radiative stabilization of the metastable complex is somewhat variable but is usually broadly in the range 10^1 to 10^3 s^{-1}. The rate coefficient k_b for redissociation of the metastable collision complex varies over many orders of magnitude, and it is this factor that leads to the variation over many orders of magnitude in the k_{assoc} rate coefficients seen in Table 5. This last microscopic rate coefficient (k_b) is largely governed in turn by two variables: the size of the system, parametrized by the number of degrees of freedom S, and the binding energy E_o. It is seen in an overall sense in Table 5 that association is greatly favored by larger size and larger binding energy of the complex. More detailed and quantitative analysis of these rate coefficients is given below.

TABLE 6: Radiative Association Rates and Efficiencies at 10 K[a]

ligand	$k_{assoc}{}^b$	$k_{inf}{}^c$	Eff[d]	R^d	excess efficiency
HC_7N	4.34E−08	4.35E−08	0.998	4.3E+02	3.2
HC_5N	9.06E−09	2.38E−08	0.38	6.1E−01	1.9
H_2CCO	1.41E−13	1.20E−08	1.2E−05	1.2E−05	1.5
CH_3COOH	5.51E−09	1.30E−08	0.42	7.4E−01	1.4
$HCOOCH_3$	2.55E−09	1.54E−08	0.17	2.0E−01	0.9
H_2CCHOH	3.86E−12	8.50E−09	4.5E−04	4.5E−04	0.9
$HCOOH$	2.65E−12	1.50E−08	1.8E−04	1.8E−04	0.7
OCO	3.0E−17	1.85E−09	1.6E−08	1.6E−8	0.6
CH_2CHCN	1.36E−10	3.60E−08	3.8E−03	3.8E−03	0.3
CH_3COCH_3	2.19E−08	2.47E−08	0.89	7.8E+00	0.2
CH_3CHO	1.53E−10	2.55E−08	6.0E−03	6.0E−03	0.2
H_2CO	3.37E−14	2.06E−08	1.6E−06	1.6E−06	0.0
$NCNH_2$	7.35E−11	4.18E−08	1.8E−03	1.8E−03	0.0
H_2O	3.29E−15	2.36E−08	1.4E−07	1.4E−07	−0.1
CH_3OCH_3	3.47E−10	1.13E−08	0.031	3.2E−02	−0.1
CH_3CH_2OH	4.7E−10	1.42E−08	0.033	3.4E−02	−0.1
CH_3CH_2CN	9.4E−09	3.39E−08	0.28	3.8E−01	−0.2
CH_3OH	1.32E−12	1.54E−08	8.6E−05	8.6E−05	−0.3
CO	8.09E−20	5.70E−10	1.4E−10	1.4E−10	−0.5
CH_3CN	1.2E−11	3.54E−08	3.4E−04	3.4E−04	−0.6
NH_3	1.48E−14	6.80E−09	2.2E−06	2.2E−06	−0.7
c-C_2H_4O	7.36E−12	1.70E−08	4.3E−04	4.3E−04	−0.7
HCN	2.08E−15	2.60E−08	8.0E−08	8.0E−08	−0.8
$HCONH_2$	2.75E−10	3.47E−08	7.9E−03	8.0E−03	−0.9
$CH_3CH_2NH_2$	1.57E−09	1.06E−08	0.15	1.7E−01	−1.2
$(CH_3)_2NH$	1.16E−09	8.30E−09	0.14	1.6E−01	−1.2
H_2CNH	2.04E−13	2.01E−08	1.0E−05	1.0E−05	−1.3
CH_3NH_2	5.59E−12	1.15E−08	4.9E−04	4.9E−04	−1.4
$HCOCH_2OH$	6.87E−09	2.13E−08	0.32	4.8E−01	−1.7

[a] In this table, the ligands are ranked in order of declining "excess efficiency", the deviation from the (logarithmic) efficiency parameter R predicted from the trend line of Figure 3. [b] Radiative association rate coefficient at 10 K from Table 5, cm^3 $molecule^{-1}$ s^{-1}. [c] High-pressure limiting rate coefficient at 10 K, cm^3 $molecule^{-1}$ s^{-1}. [d] Eff = k_{assoc}/k_{coll}; $R = k_{assoc}/(k_{coll} - k_{assoc})$. See text for discussion.

3.4. Association Efficiencies. The VTST rate coefficient calculation also provides a value for the collision rate coefficient k_{inf} (the rate coefficient at infinite pressure, which may be equated with k_f in eq 1) so that it is possible to look at the association efficiency relative to the collision rate, in addition to the absolute rate of association already displayed in Table 5. Such a tabulation of collisional efficiencies is given in column 4 of Table 6 (Eff). For the purposes of the discussion below, the reaction efficiency is also given here in terms of the "efficiency parameter" R defined as $R = k_{assoc}/(k_{coll} - k_{assoc})$. R has a value of 1 when the collisional efficiency of association is 50% and decreases as the efficiency decreases.

The principles governing association reactions of polyatomic systems (whether radiatively or collisionally stabilized) have long been understood in the context of the theory of unimolecular reaction kinetics. (See ref 78, for instance.) The most important factors influencing radiative association kinetics are the size of the system (characterized by S, the number of internal degrees of freedom of the ion−neutral collision complex), the binding energy E_o (or BDE) of the complex, the frequencies

and radiative intensities of the radiative emissions of the complex, and *T*, the temperature at which the reactant ion and neutral molecule are equilibrated prior to collision. It is of interest for future applications to look for regularities and predictive characteristics of the association kinetics results for this varied array of ligands. The kinetic effects of these various factors will be discussed briefly in light of the regularities appearing in Tables 5 and 6.

Temperature Effects. Temperature has a large effect on the rate coefficients, but this effect is largely uniform and predictable. Rates of radiative association decrease sharply with rising temperature. As a broad generality, the rate coefficients decrease by 8 times upon warming from 10 to 30 K, by 10 times on warming from 30 to 100 K, and by very roughly 15 times upon warming from 100 to 300 K. A very rough but useful generalization would be that the rate decreases by a factor of 10 for each factor of 3 increase in temperature. There are variations around these average numbers, and in addition there are two situations giving drastically reduced temperature effects. For one thing, some very small diatomics and triatomics lacking low-frequency vibrational modes (like CO, CO_2, HCN) are incapable of storing much thermal energy and exhibit much smaller than average temperature variation. Also, in a few cases (like HC_5N) the rate coefficient approaches the collision rate (saturates) with falling temperature, which leads to much smaller than average temperature variation for low temperatures.

Size and Binding Energy. For further consideration of the systematics of radiative association, the focus will be on the results at 10 K, to facilitate comparison with our previous (astrochemically motivated) studies on related systems.[23,63] In accounting for the effects of size and binding energy, it has often been noted as an empirical correlation[79] that, other things being equal, radiative association efficiencies give a remarkably accurate scaling using the parameter ($E_oS^{0.5}$). To test this possible scaling law here, it is most convenient to describe the association efficiencies using the efficiency parameter *R*, which is the reason for using this particular measure of efficiencies in Table 6. The empirical observation in various studies has been that (log *R*) is often linear in ($E_oS^{0.5}$) to a very high degree of accuracy. Figure 3 plots the log *R* values for the present data set at 10 K against this size/energy parameter. The overall fit to this expected linear correlation is good, showing that ($E_oS^{0.5}$) provides a useful correlative and predictive parameter for these radiative associations. It is notable how well this correlation stands up across such an enormous range of ligand types and sizes.

Radiative Effects. The correlation plot of Figure 3 does a reasonably good job of collapsing the wide variation of *R* values for this data set onto a linear one-dimensional scale, but there is still substantial variation. Much of the residual variation can be attributed to the varying radiative properties of the different classes of ligand molecules in this set. The linear trend line in Figure 3 predicts that

$$\log_{10} R_{\text{predicted}}\,(10\text{ K}) = 0.0118E_oS^{0.5} - 10.3 \qquad (2)$$

(with E_o in kJ mol^{-1}). Table 6 gives a re-listing of the ligands ordered according to their deviation from this predicted correlation. An "excess efficiency" value is listed in the table representing the deviation of $\log_{10} R$ from the trend line given by eq 2. It is our conclusion, as discussed below, that the molecules which associate faster than expected from the correlation of Figure 3 (that is, those with a positive excess efficiency) tend to be those with strong infrared chromophores. The deviations from the expected efficiency arising (presumably) from these radiative emission effects can increase or decrease the association efficiency by as much as about a factor of 30.

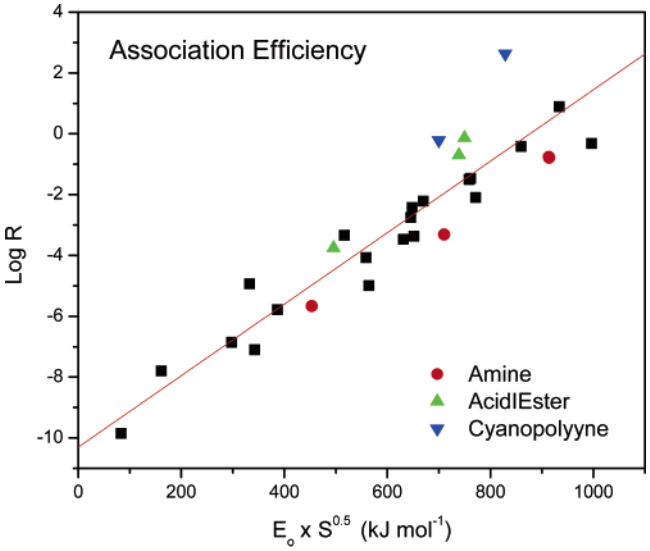

Figure 3. Plot of the logarithm of the radiative association efficiency parameter *R* against the empirically derived parameter $E_oS^{0.5}$ (from Table 6). Three particular classes of ligands are separately marked to illustrate the effect of the radiative properties of the ligand in producing exceptionally low efficiency (amines) and exceptionally high efficiency (acids/esters, and cyanopolyynes).

One simple way of rationalizing these radiative strength effects, and making sense of the ordering of Table 6, is to argue that the presence of polar unsaturated bonds and extended double-bond systems are features leading to unusually rapid infrared radiative emission and to look for a correlation of high-association-efficiency ligands with these characteristics. As a straightforward first step in establishing such a correlation, a simple division of the ligands into those containing, versus those lacking, an unsaturated bond is found to perform fairly well in predicting the high-efficiency, versus the low-efficiency, systems. Going a step farther to look in more detail at specific classes of ligands, three particularly extreme types of molecules can be singled out for illustration in Figure 3. The red symbols denote the saturated amines (having no unsaturated bonds), which all lie much below the average line. The green symbols identify the RCOOR compounds (acids and esters), containing a highly polar C═O bond, which lie well above the average. The blue symbols identify the cyanopolyacetylenes, which have polar, conjugated, extended double-bond systems, and show efficiencies far above the average line.

Overall, the regularities identified here in the temperature effects, the size/binding-energy effects, and the radiative efficiency effects, appear to account well for most of the variation of the association efficiencies across the data set. These regularities should have useful predictive value for other analogous systems of metal ion complexes with organic ligands.

3.5. Implications for Interstellar Chemistry. From the point of view of interstellar modeling it is useful to separate the ligands into three groups: those with high, more or less saturated association efficiencies, those with negligible efficiencies, and those with intermediate efficiencies. The last group is the one needing most careful quantitative analysis of the kinetics, because these intermediate ligands may or may not play a role in particular chemistries, depending on the detailed conditions and kinetic scheme of the situation at hand. Assessing the possible Mg^+-scavenging role of a ligand taken from either the high- or low-efficiency group is more straightforward in either

of these situations, because calculating the exact value of the rate coefficient is not crucial to deciding whether the reaction needs to be taken into account. Table 5 orders the ligands in order of k_{assoc} at 10 K. It is seen that the first six or seven, down to about CH_3COOH, belong to the first group in the context of low-temperature environments, where they can all be considered as high-efficiency ligands for Mg^+ scavenging. Those going downward in the table from CH_3CN constitute the second group: they always have rate coefficients more than 2 orders of magnitude below the collision rate even at very low temperature and would have negligible reaction efficiency with Mg^+ in most situations. The eight or so ligands intermediate between these ranges make up the third group, and might be candidates for important roles in the Mg^+ chemistry of some low-temperature environments.

For the high-temperature interstellar environments providing motivation for the present analysis, the assignment of the ligands into these three categories is substantially shifted. Taking the 100 K results as appropriate to such high-temperature environments, only HC_7N and CH_3COCH_3 can definitely be considered as high-efficiency Mg^+ scavengers, whereas those downward from about CH_3CH_2OH to the bottom of Table 5 seem likely to be very low in efficiency. The seven or so ligands lying between, from CH_3CH_2CN to $(CH_3)_2NH$, can be considered as intermediate cases, with potential importance in assessments of the chemistry of such warm environments.

Among the most interesting candidates for extraterrestrial chemical significance, the cyanopolyynes are well-known as potentially important partners in the metal ion chemistry of interstellar and circumstellar clouds.[23,47,63] Other molecules in the high-efficiency category have comparably fast association chemistry and could also be important Mg^+ scavengers if their neutral-molecule densities are high in a particular environment. Acetone, CH_3COCH_3, is the most efficient of these, but some others, including cyanoethane, C_2H_5CN, glycolaldehyde, $CHOCH_2OH$, and acetic acid, CH_3COOH, are also quite efficient, even at temperatures as high as 100 K.

4. Conclusion

Our calculated CP-dG2thaw Mg^+/ligand BDE values show generally good agreement with existing literature values, where available, and assist in some measure in resolving between discrepant measurements. Though the trend in BDE values to Mg^+ largely matches that found for Na^+/ligand complexes in an earlier CP-dG2thaw study, there are also indications that the two metal ions have different innate "preferences" among monodentate ligands: Na^+ bond strengths to nitriles and aldehydes are (among sodium ion complexes) comparatively high, whereas Mg^+ binds very strongly to amines and alcohols. Nevertheless, in all of the examples surveyed in this work, the BDEs for Mg^+ to polar ligands significantly exceed the analogous values for Na^+. This trend is interpreted in light of the greater tendency of Mg^+, versus Na^+, to form adducts featuring significant metal/ligand covalency.

Further subtleties are evident in the examples of bidentate ligand complexation explored here. The signal failure of chelation of Mg^+ by carboxylic acid, ester, and amide functionalities, which uniformly adopt a carbonyl-coordinated geometry, contrasts with the binding of Mg^+ to both oxygen atoms within the glycolaldehyde ligand $HCOCH_2OH$. We argue that chelation is impeded in the carboxylate- and amide-containing species due to resonance effects within these functional groups.

The kinetics of radiative association with Mg^+ across this diverse set of ligands generally follows the trends expected from other studies in terms of the dependence on temperature, ligand size and binding energy. The rates increase approximately by an order of magnitude when the temperature is lowered by a factor of 3, until at some sufficiently low temperature the association rate may saturate and become similar to the ion−neutral collision rate. The dependence of the rates on ligand size and binding energy is contained to a first approximation in the well-established empirical linear relation between $\log_{10} R$ and $E_o S^{0.5}$. Divergences of as much as a factor of 30 of the rate coefficients from this latter linear correlation are found, however, which is considered to reflect primarily the presence or absence of efficiently radiating infrared chromophoric features in the ligand molecule. It is suggested that especially large infrared radiative brightness is associated with the presence of polar unsaturated bonds, particularly when an extended polar π-bond network is formed. Because this effect is essentially a reflection of the ligand characteristics, which are largely unaffected by the predominantly electrostatic interaction between metal ion and ligand, it can be expected that similar considerations would affect the association kinetics of other main-group metal ions with the ligands surveyed here, in an analogous fashion to the behavior seen for Mg^+.

Acknowledgment. S.P. thanks the Australian Partnership of Advanced Computing, operating through the ANU Supercomputing Facility, for the generous provision of supercomputer access. R.C.D. acknowledges the support of the donors of the Petroleum Research Fund, administered by the American Chemical Society.

References and Notes

(1) Searles, S. K.; Dzidic, I.; Kebarle, P. *J. Am. Chem. Soc.* **1969**, *91*, 2810.
(2) Spears, K. G.; Fehsenfeld, F. C. *J. Chem. Phys.* **1972**, *56*, 5698.
(3) Wieting, R. D.; Staley, R. H.; Beauchamp, J. L. *J. Am. Chem. Soc.* **1975**, *97*, 924.
(4) Woodin, R. L.; Beauchamp, J. L. *J. Am. Chem. Soc.* **1978**, *100*, 501.
(5) Allison, J.; Ridge, D. P. *J. Am. Chem. Soc.* **1979**, *101*, 4998.
(6) Rodgers, M. T.; Armentrout, P. B. *J. Am. Chem. Soc.* **2000**, *122*, 8548.
(7) Ryzhov, V.; Dunbar, R. C.; Cerda, B.; Wesdemiotis, C. *J. Am. Soc. Mass Spectrom.* **2000**, *11*, 1037.
(8) Amunugama, R.; Rodgers, M. T. *J. Phys. Chem. A* **2001**, *105*, 9883.
(9) Gapeev, A.; Dunbar, R. C. *J. Am. Chem. Soc.* **2001**, *123*, 8360.
(10) Rodgers, M. T.; Armentrout, P. B. *J. Am. Chem. Soc.* **2002**, *124*, 2678.
(11) Hoyau, S.; Norrman, K.; McMahon, T. B.; Ohanessian, G. *J. Am. Chem. Soc.* **1999**, *121*, 8864.
(12) Amicangelo, J. C.; Armentrout, P. B. *J. Phys. Chem. A* **2000**, *104*, 11420.
(13) Armentrout, P. B.; Rodgers, M. T. *J. Phys. Chem. A* **2000**, *104*, 2238.
(14) Burk, P.; Koppel, I. A.; Koppel, I.; Kurg, R.; Gal, J. F.; Maria, P. C.; Herreros, M.; Notario, R.; Abboud, J. L. M.; Anvia, F.; Taft, R. W. *J. Phys. Chem. A* **2000**, *104*, 2824.
(15) McMahon, T. B. *Int. J. Mass Spectrom.* **2000**, *200*, 187.
(16) Amicangelo, J. C.; Armentrout, P. B. *Int. J. Mass Spectrom.* **2001**, *212*, 301.
(17) Steel, E. A.; Merz, K. M.; Selinger, A.; Castleman, A. W. *J. Phys. Chem.* **1995**, *99*, 7829.
(18) Laidig, K. E.; Speers, P.; Streitwieser, A. *Coord. Chem. Rev.* **2000**, *197*, 125.
(19) Niedner-Schattenburg, G.; Bondybey, V. E. *Chem. Rev.* **2000**, *100*, 4059.
(20) Smith, D.; Adams, N. G.; Alge, E.; Herbst, E. *Astrophys. J.* **1983**, *272*, 365.
(21) Boissel, P. *Astron. Astrophys.* **1994**, *285*, L33.
(22) Petrie, S.; Becker, H.; Baranov, V. I.; Bohme, D. K. *Astrophys. J.* **1997**, *476*, 191.
(23) Petrie, S.; Dunbar, R. C. *J. Phys. Chem. A* **2000**, *104*, 4480.
(24) Petrie, S. *J. Phys. Chem. A* **2001**, *105*, 9931.
(25) Petrie, S. *J. Phys. Chem. A* **2002**, *106*, 5188.

(26) Bauschlicher, C. W.; Sodupe, M.; Partridge, H. *J. Chem. Phys.* **1992**, *96*, 4453.
(27) Sodupe, M.; Bauschlicher, C. W. *Chem. Phys. Lett.* **1992**, *195*, 494.
(28) Willey, K. F.; Yeh, C. S.; Robbins, D. L.; Pilgrim, J. S.; Duncan, M. A. *J. Chem. Phys.* **1992**, *97*, 8886.
(29) Yeh, C. S.; Willey, K. F.; Robbins, D. L.; Pilgrim, J. S.; Duncan, M. A. *Chem. Phys. Lett.* **1992**, *196*, 233.
(30) Watanabe, H.; Iwata, S.; Hashimoto, K.; Misaizu, F.; Fuke, K. *J. Am. Chem. Soc.* **1995**, *117*, 755.
(31) Asada, T.; Iwata, S. *Chem. Phys. Lett.* **1996**, *260*, 1.
(32) Trachtman, M.; Markham, G. D.; Glusker, J. P.; George, P.; Bock, C. W. *Inorg. Chem.* **1998**, *37*, 4421.
(33) Chen, Q.; Milburn, R. K.; Hopkinson, A. C.; Bohme, D. K.; Goodings, J. M. *Int. J. Mass Spectrom.* **1999**, *184*, 153.
(34) Andersen, A.; Muntean, F.; Walter, D.; Rue, C.; Armentrout, P. B. *J. Phys. Chem. A* **2000**, *104*, 692.
(35) Operti, L.; Tews, E. C.; Freiser, B. S. *J. Am. Chem. Soc.* **1988**, *110*, 3847.
(36) Yeh, C. S.; Willey, K. F.; Robbins, D. L.; Duncan, M. A. *Int. J. Mass Spectrom. Ion Processes* **1994**, *131*, 307.
(37) France, M. R.; Pullins, S. H.; Duncan, M. A. *Chem. Phys.* **1998**, *239*, 447.
(38) Lu, W.; Yang, S. H. *J. Phys. Chem. A* **1998**, *102*, 825.
(39) Milburn, R. K.; Baranov, V. I.; Hopkinson, A. C.; Bohme, D. K. *J. Phys. Chem. A* **1998**, *102*, 9803.
(40) Shoeib, T.; Milburn, R. K.; Koyanagi, G. K.; Lavrov, V. V.; Bohme, D. K.; Siu, K. W. M.; Hopkinson, A. C. *Int. J. Mass Spectrom.* **2000**, *201*, 87.
(41) Milburn, R. K.; Bohme, D. K.; Hopkinson, A. C. *THEOCHEM* **2001**, *540*, 5.
(42) Yoshida, S.; Okai, N.; Fuke, K. *Chem. Phys. Lett.* **2001**, *347*, 93.
(43) Yeh, C. S.; Pilgrim, J. S.; Willey, K. F.; Robbins, D. L.; Duncan, M. A. *Int. Rev. Phys. Chem.* **1994**, *13*, 231.
(44) Kawaguchi, K.; Kagi, E.; Hirano, T.; Takano, S.; Saito, S. *Astrophys. J.* **1993**, *406*, L39.
(45) Guelin, M.; Lucas, R.; Cernicharo, J. *Astron. Astrophys.* **1993**, *280*, L19.
(46) Highberger, J. L.; Savage, C.; Bieging, J. H.; Ziurys, L. M. *Astrophys. J.* **2001**, *562*, 790.
(47) Petrie, S. *Mon. Not. R. Astron. Soc.* **1996**, *282*, 807.
(48) Miao, Y. T.; Mehringer, D. M.; Kuan, Y. J.; Snyder, L. E. *Astrophys. J.* **1995**, *445*, L59.
(49) Kuan, Y. J.; Snyder, L. E. *Astrophys. J.* **1996**, *470*, 981.
(50) Nummelin, A.; Bergman, P.; Hjalmarson, A.; Friberg, P.; Irvine, W. M.; Millar, T. J.; Ohishi, M.; Saito, S. *Astrophys. J. Suppl. Ser.* **2000**, *128*, 213.
(51) Charnley, S. B.; Ehrenfreund, P.; Kuan, Y. J. *Spectrochim. Acta A* **2001**, *57*, 685.
(52) Walmsley, C. M.; Bachiller, R.; Pineau des Forets, G.; Schilke, P. *Astrophys. J.* **2002**, *566*, L109.
(53) Furuya, R. S.; Walmsley, C. M.; Nakanishi, K.; Schilke, P.; Bachiller, R. *Astron. Astrophys.* **2003**, *409*, L21.
(54) Petrie, S. In *Chemistry as a Diagnostic of Star Formation*; Curry, C. L.; Fich, M., Eds.; NRC Research Press: Ottawa, ON, 2003; p 384.
(55) Becke, A. D. *J. Chem. Phys.* **1993**, *98*, 5648.
(56) Lee, C.; Yang, W.; Parr, R. G. *Phys. Rev. B* **1988**, *37*, 785.
(57) Curtiss, L. A.; Raghavachari, K.; Trucks, G. W.; Pople, J. A. *J. Chem. Phys.* **1991**, *94*, 7221.
(58) Petrie, S. *J. Phys. Chem. A* **1998**, *102*, 6138.
(59) Siu, F. M.; Ma, N. L.; Tsang, C. W. *J. Chem. Phys.* **2001**, *114*, 7045.
(60) Petrie, S. *J. Phys. Chem. A* **2002**, *106*, 7034.
(61) Frisch, M. J.; Trucks, G. W.; Schegel, H. B.; Scuseria, G. E.; Robb, M. A.; Cheeseman, J. R.; Zakrzewski, V. G.; Montgomery, J. A., Jr.; Stratmann, R. E.; Burant, J. C.; Dapprich, S.; Millam, J. M.; Daniels, A. D.; Kudin, K. N.; Strain, M. C.; Farkas, O.; Tomasi, J.; Barone, V.; Cossi, M.; Cammi, R.; Mennucci, B.; Pomelli, C.; Adamo, C.; Clifford, S.; Ochterski, J. W.; Petersson, G. A.; Ayala, P. Y.; Cui, Q.; Morokuma, K.; Malick, D. K.; Rabuck, A. D.; Raghavachari, K.; Foresman, J. B.; Cioslowski, J.; Ortiz, J. V.; Stefanov, B. B.; Liu, G.; Liashenko, A.; Piskorz, P.; Komaromi, I.; Gomperts, R.; Martin, R. L.; Fox, D. J.; Keith, T.; Al-Laham, M. A.; Peng, C. Y.; Nanayakkara, A.; Gonzalez, C.; Challacombe, M.; Gill, P. M. W.; Johnson, B. G.; Chen, W.; Wong, M. W.; Andres, J. L.; Head-Gordon, M.; Replogle, E. S.; Pople, J. A. *Gaussian98*, rev. A.7; Gaussian, Inc.: Pittsburgh, PA, 1998.
(62) Klippenstein, S. J.; Yang, Y.-C., Ryzhov, V.; Dunbar, R. C. *J. Chem. Phys.* **1996**, *104*, 4502.
(63) Dunbar, R. C.; Petrie, S. *Astrophys. J.* **2002**, *564*, 792.
(64) Klippenstein, S. J.; Wagner, A. F.; Dunbar, R. C.; Wardlaw, D. M.; Robertson, S. H.; Diau, E. W. VariFlex computer code, available via anonymous FTP from london.tcg.anl.gov.
(65) Although the smallest O-containing ligand, H_2O, exhibits the smallest BDE discrepancy, of 2.1 kJ mol^{-1}, between the two methods, there is no apparent systematic dependence of the discrepancy on either ligand size or position upon the BDE "ladder". Although several larger O-containing ligands have both significantly larger BDE values and larger discrepancies than those seen for H_2O, the largest discrepancy (of 11.2 kJ mol^{-1}) is seen for the ketene molecule H_2CCO which has, according to both methods, a BDE value much lower than that of H_2O.
(66) Dalleska, N. F.; Tjelta, B. L.; Armentrout, P. B. *J. Phys. Chem.* **1994**, *98*, 4191.
(67) Yeh, C. S.; Willey, K. F.; Robbins, D. L.; Pilgrim, J. S.; Duncan, M. A. *J. Chem. Phys.* **1993**, *98*, 1867.
(68) Bauschlicher, C. W.; Partridge, H. *J. Phys. Chem.* **1991**, *95*, 3946.
(69) The preference for carbonyl or nitrile coordination, over the NH_2 site in $HCONH_2$ and H_2NCN, is at odds with the trend in BDEs to the simplest carbonyl-, nitrile-, and amine-containing ligands H_2CO, HCN, and NH_3 (see Table 1). This propensity, for $HCONH_2$ carbonyl-centred coordination to several metal ions including Mg^+, has been explored previously by Tortajada et al.[70] whose G2(MP2) binding energy of 203 kJ mol^{-1} compares favorably with our CP-dG2thaw value but markedly exceeds our CP-MP2 value. Tortajada et al.[70] contend that the carbonyl coordination preferred in the formamide complex with Mg^+ (and Li^+, Na^+, and Al^+) arises through maximization of the ion/dipole interaction.
(70) Tortajada, J.; Leon, E.; Morizur, J.-P.; Luna, A.; Mó, O.; Yáñez, M. *J. Phys. Chem.* **1995**, *99*, 13890.
(71) McMahon, T. B.; Ohanessian, G. *Chem. Eur. J.* **2000**, *6*, 2931.
(72) Petrie, S. *Int. J. Mass Spectrom.* **2003**, *227*, 33.
(73) Petrie, S. *J. Phys. Chem. A* **2003**, *107*, 10441.
(74) Bader, R. F. W. *Atoms in Molecules: A Quantum Theory*; Oxford University Press: Oxford, U.K., 1990.
(75) Nelson, R. D.; Lide, D. R.; Maryott, A. A. *Selected Values of Electric Dipole Moments for Molecules in the Gas Phase*; Natl. Stand. Ref. Data Ser.; Natl. Bur. Stnds. Gaithersburg, MD, 1967.
(76) Maryott, A. A.; Buckley, F. *U.S. Natl. Bur. Stnds. Circular* **1953**, *537*.
(77) Kagawa, H.; Ichimura, A.; Kamka, N. A.; Mori, K. *J. Mol. Struct. (THEOCHEM)* **2001**, *546*, 127.
(78) Holbrook, K. A.; Pilling, M. J.; Robertson, S. H., *Unimolecular Reactions*; Wiley: New York, 1996.
(79) Dunbar, R. C. Ion−Molecule Radiative Association. In *Current Topics in Ion Chemistry and Physics*; Ng, C. Y.; Baer, T.; Powis, I., Eds.; Wiley: New York, 1994; Vol. II, pp 279−335.